1995RMxAA..31...51R

Revista Mexicana de Astronomía y Astrofísica, **31**, 51-61 (1995)

THE INITIAL STAGES OF AN HH JET/CLOUD CORE COLLISION

A.C. Raga and J. Cantó

Instituto de Astronomía
Universidad Nacional Autónoma de México

Received 1995 January 31

RESUMEN

Presentamos un estudio de la evolución inicial de la colisión de un jet HH (Herbig-Haro) con una nube molecular densa. Un modelo analítico sencillo muestra que la interacción resulta en un jet reflejado de menor colimación para un amplio rango de ángulos de incidencia del jet. Usamos simulaciones numéricas bidimensionales de la interacción de jets de fuentes con velocidad constante o variable con nubes de alta densidad (con cocientes de densidades de la nube/jet infinitos) para comprobar la validez de nuestro modelo analítico y también para mostrar el efecto de la colisión jet/nube sobre las superficies de trabajo internas (que resultan de la velocidad variable de la fuente). Describimos asimismo predicciones de mapas de emisión en [S II] de estos modelos. Finalmente, presentamos simulaciones numéricas de interacciones jet/nube con cocientes de densidades nube/jet finitos y discutimos las implicaciones observacionales de estos modelos.

ABSTRACT

We present a study of the initial evolution of the collision of an HH (Herbig-Haro) jet with a dense molecular cloud core. A simple analytical model shows that for a wide range of angles of incidence of the jet, the interaction will result in the formation of a reflected, less well collimated jet beam. Two-dimensional numerical simulations of the interaction of jets from constant and variable velocity sources with high density clouds (i.e., with infinite cloud-to-jet density ratios) are used to check the simple analytical model, and also to show the effect of the jet/cloud collision on the evolution of the internal working surfaces (formed by the source velocity variability). Predictions of [S II] emission maps from these models are also discussed. Finally, we present numerical simulations of jet/cloud interactions with finite cloud-to-jet density ratios, and discuss the observational implications of these models.

Key words: **HYDRODYNAMICS — ISM – JETS AND OUTFLOWS**

1. INTRODUCTION

HH (Herbig-Haro) jets have traditionally been interpreted in terms of the theoretical framework developed for laboratory jets. The structure of such flows is determined by the interaction of the jet with the surrounding environment, which can take place at the head of the jet (through the formation of a Mach disk and a bowshock), or along the outer surface of the beam of the jet (with jet/environment pressure differences driving recollimation shocks into the beam, or Kelvin-Helmholtz instabilities giving rise to turbulent boundary layers; see Cantó & Raga 1991).

It has recently been realized that many of the structures seen in HH jets might actually be quite different from the ones observed in laboratory jets. In particular, it is now thought that the morphology of many HH jets might at least partly be the direct result of a time-variability of the source ejection, rather than an effect of the jet/environment interaction by itself. Different morphologies can be explained quite straightforwardly in terms of a variability in the magnitude of the ejection velocity, the

© Universidad Nacional Autónoma de México • Provided by the NASA Astrophysics Data System

1995RMxAA..31...51R

ejection direction, or a combined velocity+direction variability (see the review of Raga 1993, and references therein).

These models stress the differences between laboratory jets (which are ejected from stable, rigid sources) and HH jets (which may have time-variable sources). However, the basic jet/environment interaction mechanisms seen in laboratory jets also have to be present in HH jets, even if they might not play a deciding role on producing the observed morphologies of HH jets. In the present paper, we discuss the very drastic jet/environment interaction that occurs when an HH jet runs into a high density obstacle (e.g., a molecular cloud core). Such interactions lead either to a sudden deflection, or to the destruction of the jet beam, and might be observed in some HH objects.

As the observed radii of HH jets ($\sim 10^{14}$–10^{15} cm) are much smaller than the typical sizes of molecular cloud cores ($\sim 10^{16}$–10^{17} cm) we model the cloud core as a plane-parallel, high density "obstacle" against which the jet impacts at a given incidence angle θ. This problem allows a simplified, analytic approach which we describe in § 2.

We then present (in § 3) numerical simulations of nonadiabatic jets impacting against a rigid wall. This problem is equivalent to a jet/cloud collision for the limit of $\rho_c/\rho_j \rightarrow \infty$ (where ρ_c and ρ_j are the cloud core and jet densities, respectively). Section 4 discusses similar calculations, but for jets ejected from sources with a variable ejection velocity. Finally, in § 5 we present simulations of jet/cloud collisions with finite ρ_c/ρ_j. The results are summarized in § 6.

2. AN ANALYTIC JET/CLOUD INTERACTION MODEL

Let us consider the collision of a jet with a dense cloud. We will assume that $r_c \gg r_j$ (where r_c and r_j are the cloud and jet radii, respectively), so that the cloud effectively is a "flat" obstacle in the path of the jet, that $\rho_c \gg \rho_j$ (where ρ_c and ρ_j are the cloud and jet densities, respectively), and that the transition between the dense cloud and the surrounding, low density environment is infinitely sharp. Furthermore, we will assume that the jet initially has a very low temperature (and therefore, a very high Mach number) and that it is a parallel, perfectly collimated "slab jet".

The initial shock structure that will arise in the region of impact is shown in Figure 1. The jet impacts at a velocity v_j and an incidence angle θ on the horizontal cloud/environment boundary. A shock S_1 (at an angle α with the unperturbed cloud/environment boundary) deflects the material of the jet to a direction parallel with the cloud/environment boundary. The high pressure behind the shock S_1 then pushes a second shock S_2 into the cloud (see Figure 1).

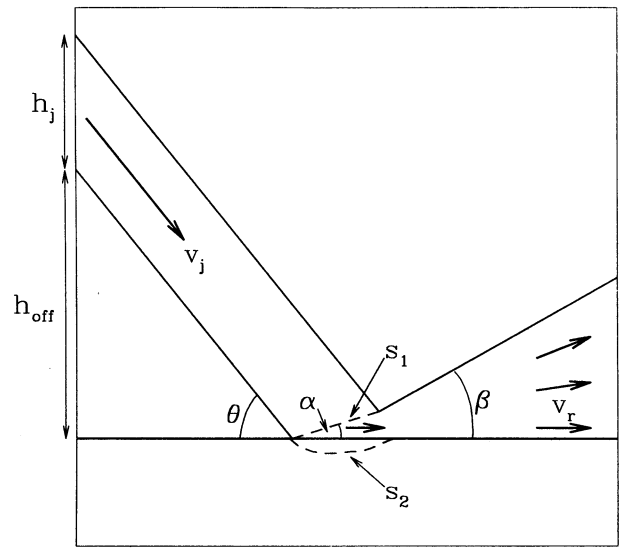

Fig. 1. Schematic diagram showing a jet beam of velocity v_j that impinges at an angle θ on the surface of a dense cloud (represented by the thick, horizontal line). The initially perfectly collimated beam is deflected onto a direction roughly parallel to the surface of the cloud, and emerges from the collision region with a nonzero opening angle β and a reduced velocity v_r. Two shocks are generated in the collision region: the $S1$ shock in the jet beam (at an angle α to the unperturbed cloud surface), and the $S2$ shock moving into the dense cloud. The parameters h_j and h_{off} shown in this diagram are used to specify the characteristics of the numerical simulations (see Table 1).

If we assume that both shocks (S_1 and S_2) are strong, the requirement of post-shock pressure balance directly implies that:

$$v_2 = \sqrt{\frac{\rho_j}{\rho_c}}\, v_1 \,, \qquad (1)$$

where v_1 and v_2 are the shock velocities of the S_1 and S_2 shocks (respectively). In order to be able to proceed analytically, we note that as we necessarily have $v_1 \leq v_j$, for the $\rho_c \gg \rho_j$ case that we are considering, we have $v_2 \ll v_j$. So, in the limit of very high cloud core densities, the shock S_2 travels into the cloud at very low velocities, so that the cloud/environment surface is deformed at a very slow rate. In this limit, we can then assume that the surface of the dense cloud effectively behaves as a rigid obstacle.

Under these conditions, the jet/cloud core collision simplifies to the problem of a jet impacting on a flat, rigid surface. This problem has been studied analytically in considerable detail by Cantó, Tenorio-

© Universidad Nacional Autónoma de México • Provided by the NASA Astrophysics Data System

1995RMxAA..31...51R

Tagle, & Różyczka (1988), and our following discussion is almost directly based on their results. We will furthermore restrict ourselves to the strongly radiative case, in which one assumes that the gas behind the S_1 shock instantaneously cools to an "equilibrium temperature" $T_{eq} \sim 10^4$ K.

For this highly radiative case, it is possible to show that the S_1 shock is planar, and that its angle α with respect to the cloud surface (see Figure 1) is given by

$$\tan\alpha \approx \frac{(kT_{eq}/m)}{{v_j}^2 \sin\theta \cos\theta}, \qquad (2)$$

where m is the average mass per particle. It is also possible to show (see Cantó et al. 1988) that the S_1 shock velocity v_1 is given by

$$v_1 \approx v_j \sin\theta, \qquad (3)$$

and that the velocity of the jet beam before (v_j) and after (v_r, see figure 1) the jet/cloud impact obey the relation

$$v_r \approx v_j \cos\theta. \qquad (4)$$

Therefore, the effect of the jet/cloud interaction is to increase the temperature (from the initial jet temperature up to T_{eq}) and to decrease the velocity (from v_j to v_r) of the jet beam, resulting in a decrease of the Mach number of the jet. From equation (4), it is clear that a fraction $(1 - \sin^2\theta)$ of the initial kinetic energy of the jet is lost in the collision. As the region behind the S_1 shock is highly overpressured, the material leaving the impact region will start to expand in a Mach cone of angle β, given by

$$\sin\beta \approx \frac{2}{(\gamma - 1)\, M_{eq} \cos\theta}, \qquad (5)$$

where

$$M_{eq} = \frac{v_j}{\sqrt{\gamma k T_{eq}/m}} \qquad (6)$$

is the Mach number of the incident jet with respect to the sound speed at the equilibrium temperature T_{eq} (with γ being the specific heat ratio, see Cantó,

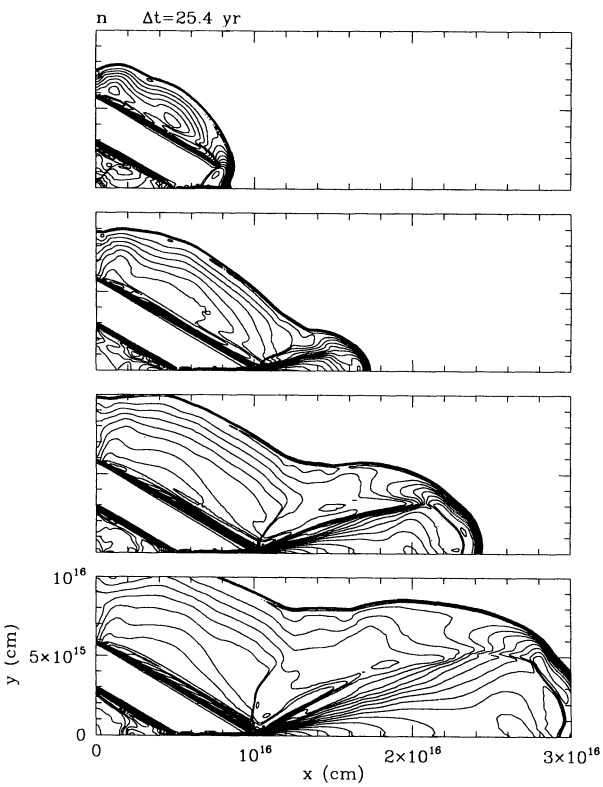

Fig. 2. Time-sequence of the density stratification for Model 1 (see the text and Table 1). The successive frames are taken at time-intervals of 25.4 yr from the beginning of the numerical integration. The logarithmic contours correspond to factors of $\sqrt{2}$.

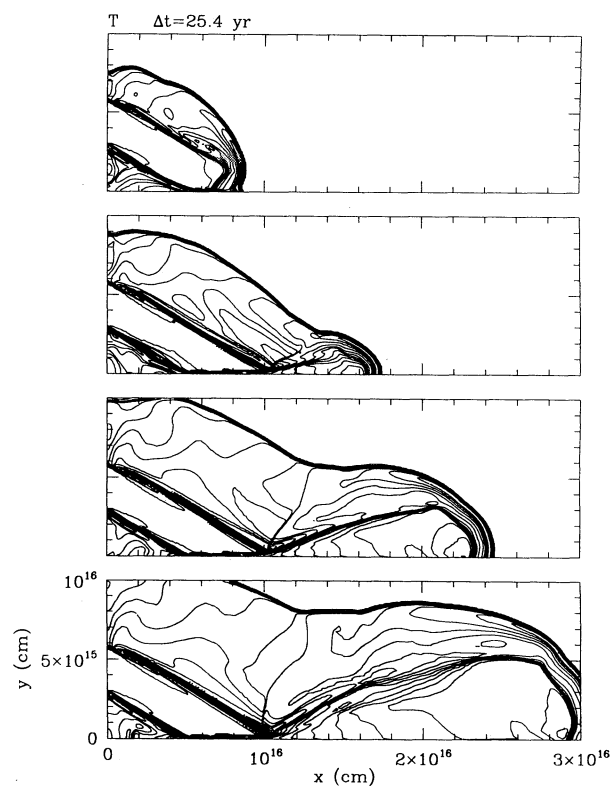

Fig. 3. Time-sequence of the temperature stratification for Model 1 (see the text and Table 1). The successive frames are taken at the same time-intervals as in Figure 2. The logarithmic contours correspond to factors of $\sqrt{2}$.

© Universidad Nacional Autónoma de México • Provided by the NASA Astrophysics Data System

1995RMxAA..31...51R

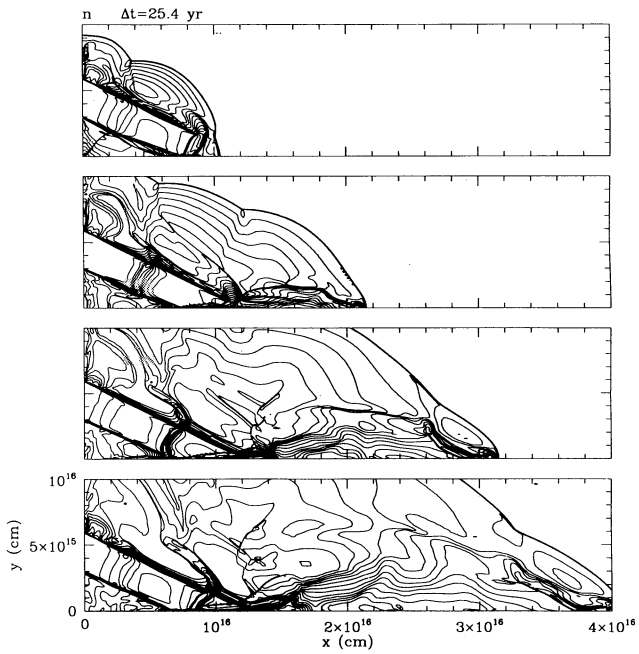

Fig. 4. Time-sequence of the density stratification for Model 2 (see the text and Table 1). The successive frames are taken at time-intervals of 25.4 yr from the beginning of the numerical integration. The logarithmic contours correspond to factors of $\sqrt{2}$.

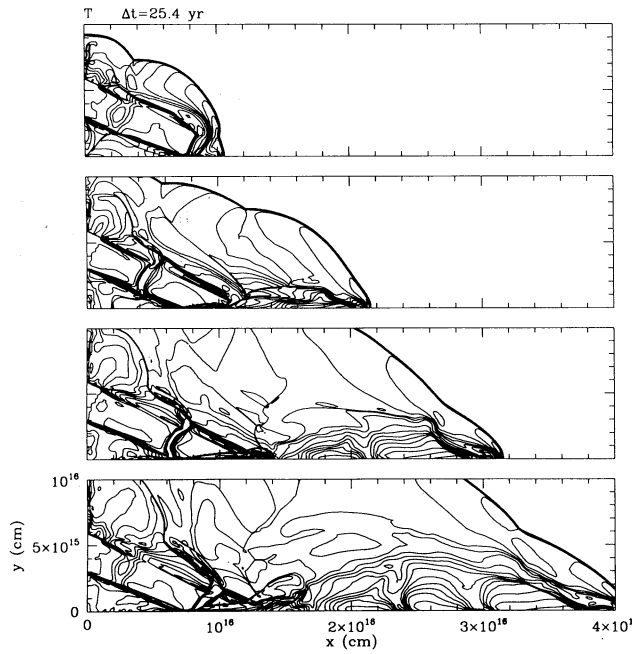

Fig. 5. Time-sequence of the temperature stratification for Model 2 (see the text and Table 1). The successive frames are taken at the same time-intervals as in Figure 4. The logarithmic contours correspond to factors of $\sqrt{2}$.

TABLE 1

MODEL PARAMETERS FOR THE NUMERICAL SIMULATIONS

Model	1	2[a]	3	4
v_j (km s^{-1})	100	100	100	100
n_j (cm^{-3})	30	6.0	5.0	5.0
n_e (cm^{-3})	1.0	0.2	0.5	0.5
n_c (cm^{-3})	∞	∞	5000	500
T_j (K)	1000	1000	1000	1000
T_e (K)	1000	1000	10000	10000
T_c (K)	...	...	1.0	10.0
θ (°)	30	25	25	25
h_j (10^{15} cm)	3.0	3.0	3.0	3.0
h_{off} (10^{15} cm)	3.0	3.0	2.0	2.0
d_{bs}/h_j	0.8	4.2	1.7	1.7
d_{coll}/h_j	0.04	0.2	0.2	0.2
x_{max} (10^{16} cm)	4.0	4.0	3.0	3.0
y_{max} (10^{16} cm)	1.0	1.0	1.5	1.5
$Nx \times Ny$	513 × 129	1025 × 257	513 × 257	513 × 257[b]
p	4	5	4	4

[a] This model has a source velocity time variability of half-amplitude $\Delta v_j = 20$ km s^{-1} and period $\tau = 19.03$ yr .

[b] For integration times larger than 100 yr, the resolution of this model was increased to 1025 × 513.

© Universidad Nacional Autónoma de México • Provided by the NASA Astrophysics Data System

1995RMxAA..31...51R

Raga, & Binette 1989). In this way, the jet/cloud interaction not only results in a deflection of the jet, but also reduces the collimation of the jet beam.

This reduction of collimation can be quite drastic, and can cause the complete destruction of the jet beam. It can be straightforwardly shown that for $\theta > \theta_c$, where (to first order in $1/M_{eq}$)

$$\theta_c \approx \frac{\pi}{2} - \frac{1}{M_{eq}}, \qquad (7)$$

the flow after the S_1 shock is subsonic. In this regime, the jet beam will not expand into a Mach cone (see equation 5), but instead will escape from the jet/cloud interaction region in all directions, resulting in a complete disruption of the jet beam. As for HH jets we have values $M_{eq} \sim 10$–30, we see that only very frontal ($\theta \approx \pi/2$) collisions with obstacles will actually result in a complete disruption of these jets.

In the following section, we present a comparison of these results with time-dependent "slab jet" numerical simulations.

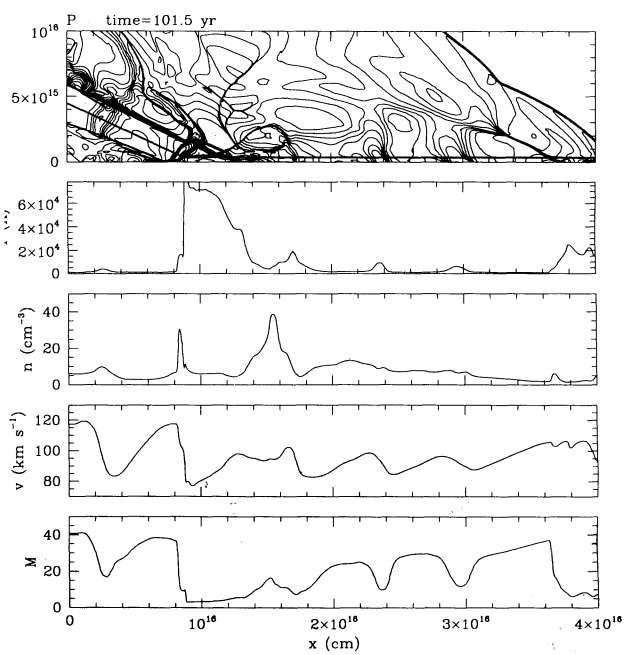

Fig. 6. The top diagram represents the pressure stratification (factor of $\sqrt{2}$ contours) of Model 2 (see the text and Table 1) corresponding to a time-integration of $t = 101.5$ yr. The lower diagrams show several flow variables (temperature, density, velocity magnitude and Mach number) as a function of x taken along a cut (represented by the thick line on the pressure stratification map) that is initially parallel to the direction of the incident jet beam, and becomes parallel to the x-axis downstream of the $S1$ shock (see Figure 1).

3. NUMERICAL SIMULATION OF THE IMPACT OF A JET AGAINST A RIGID WALL

In this section we present the results from a time-dependent, 2-D, "slab jet" numerical simulation carried out with the non-equilibrium ionization, adaptive grid Coral code (described by Raga 1994; Raga et al. 1995). A jet directed at an angle θ towards the x-axis and with top-hat density, temperature and velocity cross sections is injected between $y = h_{off}$ and $y = h_{off} + h_j$ from the left of the computational domain (see Figure 1). The cloud core/environment boundary is introduced as a reflection condition along the x-axis of the computational domain.

The simulation described in this section (Model 1, see Table 1) has a jet of velocity $v_j = 100$ km s^{-1}, density $n_j = 30$ cm^{-3}, temperature $T_j = 1000$ K and width $h_j = 3 \times 10^{15}$ cm, entering the computational domain at a height $h_{off} = 3 \times 10^{15}$ cm (see Figure 1) at an angle $\theta = 30°$ towards the x-axis. The initially stationary environment has a density $n_e = 1$ cm^{-3} and a temperature $T_e = 1000$ K. The ionization fraction of hydrogen has been assigned an initial value of 10^{-4} for both the jet and the environment. The computation has been done on a grid of spatial extent $x_{max} = 4 \times 10^{16}$ cm and $y_{max} = 10^{16}$ cm along the x- and y-axes (respectively), with $p = 4$ levels of grid refinement, and a maximum resolution (in the finest grid) of $Nx \times Ny = 512 \times 128$ grid points (see Table 1). A reflection condition is applied at the bottom boundary, as well as on the left boundary above and below the jet beam (see Figure 1). An outflow condition is applied at the top and right boundaries of the computational domain.

With these parameters, we obtain a cooling distance $d_{bs} \approx 0.8\, h_j$ (where h_j is the width of the jet, see above) behind the leading bowshock and, more importantly, a cooling distance $d_{coll} \approx 0.04\, h_j$ behind the S_1 collision shock (see Figure 1). This shows that the jet/cloud collision is indeed in a radiative regime. For these estimates of the cooling distances we have used the simple interpolation formulae derived by Cantó et al. (1988).

In Figures 2 and 3, we show a density and temperature time-sequence (respectively) obtained from this numerical simulation. One can direcly see the jet initially travelling towards the x-axis, and then being deflected through a shock that lies very close to the reflecting surface. From the numerical simulation, we can measure the angle between this shock and the x-axis, to obtain a value $\alpha_{num} \approx 1.6°$.

This result compares well with the value $\alpha \approx 1.2°$ obtained from equation (2) taking $T_{eq} = 10^4$ K and $m = 1.3\, m_H$ (where m_H is the mass of the hydrogen atom, which would be valid for a completely neutral postshock gas). The small difference between the "numerical" and "analytical" values of the angle α

© Universidad Nacional Autónoma de México • Provided by the NASA Astrophysics Data System

1995RMxAA..31...51R

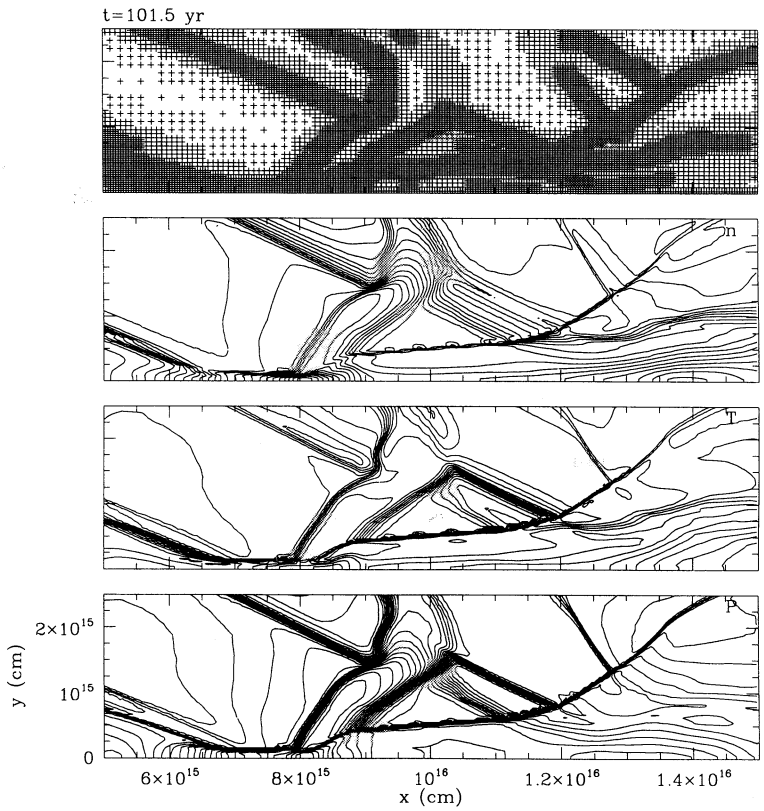

Fig. 7. Blow-up of the jet/cloud interaction region showing the stratification obtained from Model 2 for a time-integration of $t = 101.5$ yr. From top to bottom: the computational grid resulting from the adaptive grid algorithm, and the density, temperature and pressure stratifications. The logarithmic contours correspond to factors of $\sqrt{2}$.

(see Figure 1) can be accounted by the fact that the gas behind the S_1 shock exits the collision region with a temperature somewhat higher than 10^4 K, and with a non-zero ionization fraction.

It is also interesting to note that the opening angle β for the post-collision jet beam obtained from our numerical simulation has a value $\beta_{num} \approx 14°$. This result again compares well with the value $\beta \approx 20°$ obtained from our analytic formulation (setting $T_{eq} = 10^4$ K and $m = 1.3\, m_H$ in equations 5 and 6).

From the numerical simulation, one clearly sees that the jet does become less collimated as a result of the impact with an obstacle. However, the beam of the jet is preserved, and the jet still pushes a working surface into the surrounding environment. In the following section we explore numerically the interaction of internal working surfaces in the jet beam with an obstacle.

4. THE EFFECT OF A SOURCE VELOCITY VARIABILITY

In this section we discuss the results from a simulation with parameters similar to the ones of Model 1 (see § 3 and Table 1). However, in Model 2 (see Table 1) we also introduce a sinusoidal variability of the ejection velocity, with a mean value $v_j = 100$ km s^{-1}, a half-amplitude $\Delta v_j = 20$ km s^{-1}and period of oscillation $\tau = 19.0$ yr. The remaining parameters of Model 2 are listed in Table 1.

As discussed, e.g., by Raga et al. (1990) and Raga (1993), a source velocity variability with a supersonic amplitude leads to the formation of two-shock "internal working surfaces" that travel down the jet beam. The formation of such working surfaces can clearly be seen in the density and temperature time-sequences obtained from our simulation, which are shown in Figures 4 and 5 (respectively).

© Universidad Nacional Autónoma de México • Provided by the NASA Astrophysics Data System

1995RMxAA..31...51R

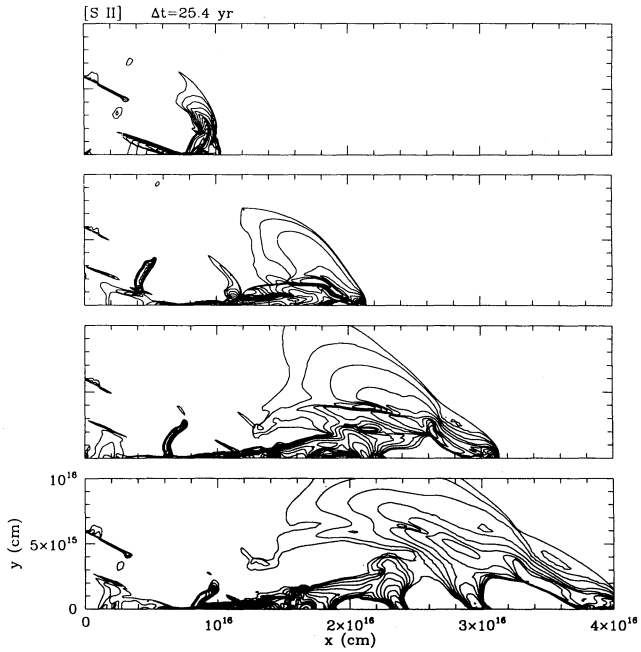

Fig. 8. Time-sequence showing the evolution of the [S II] 6717+31 emission coefficient obtained from Model 2. The successive frames are taken at the same time-intervals as in Figure 4. The logarithmic contours correspond to factors of 2.

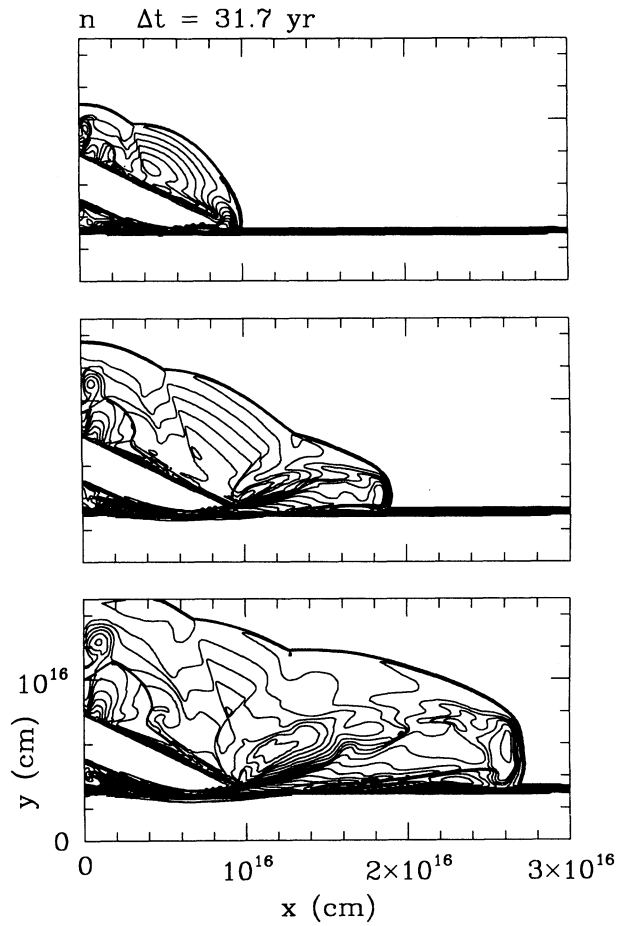

Fig. 9. Time-sequence of the density stratification for Model 3 (see the text and Table 1). The successive frames are taken at time-intervals of 31.7 yr from the beginning of the numerical integration. The logarithmic contours correspond to factors of $\sqrt{2}$.

In the region between the source and the point of the jet/cloud collision, regions of high density are formed inside the jet beam, which steepen into two-shock structures farther away from the source. These two-shock internal working surfaces are seen to push a bowshock into the surrounding medium (as predicted analytically by Raga et al. 1990, and also seen in numerical simulations such as the ones of Stone & Norman 1993).

If we calculate the cooling distance behind the $S1$ reflection shock (see Figure 1) using the average injection velocity (v_j = 100 km s^{-1}) and the initial jet density (n_j = 6 cm^{-3}, see Table 1), we obtain a value $d_{coll} \approx 0.2\,h_j$. However, the fact that the velocity along the jet beam has a velocity range between $\approx$ 80–120 km s^{-1}(see Figure 6), implies a very substantial variation in the cooling distance. Also, as can be clearly seen from Figure 6, the density along the beam of the jet also shows substantial variations, with the higher densities corresponding to the region in between the internal working surface shock pairs.

Taking into account these velocity and density variations, we can estimate a range for the cooling distance behind the $S1$ shock of $d_{coll} \approx 0.2$–$0.5\,h_j$ for the continuous segments of the jet beam. However, for the high density material in the internal working surfaces, the post-$S1$ shock cooling distance has a considerably smaller value of $d_{coll} \approx 0.04\,h_j$. From this, we see that the $S1$ shock is only marginally radiative when the continuous beam segments are going through this shock. However, the $S1$ shock is indeed highly radiative when an internal working surface is going through this shock.

A blow-up of the jet/cloud collision region (Figure 7) shows that the $S1$ reflection shock (also see Figure 1) instead of being straight now shows a complex, curved structure. The slope of the $S1$ shock has values in the range $\alpha_{num} \approx 1$–$7°$. It is interesting to note that these limits approximately correspond to the value $\alpha \approx 1.3°$ obtained from equation (2), and the value $\alpha \approx 10°$ that would be expected for an adiabatic jet/cloud collision (see Cantó et al. 1988).

The time-sequences of Figures 4 and 5 show that

© Universidad Nacional Autónoma de México • Provided by the NASA Astrophysics Data System

1995RMxAA..31...51R

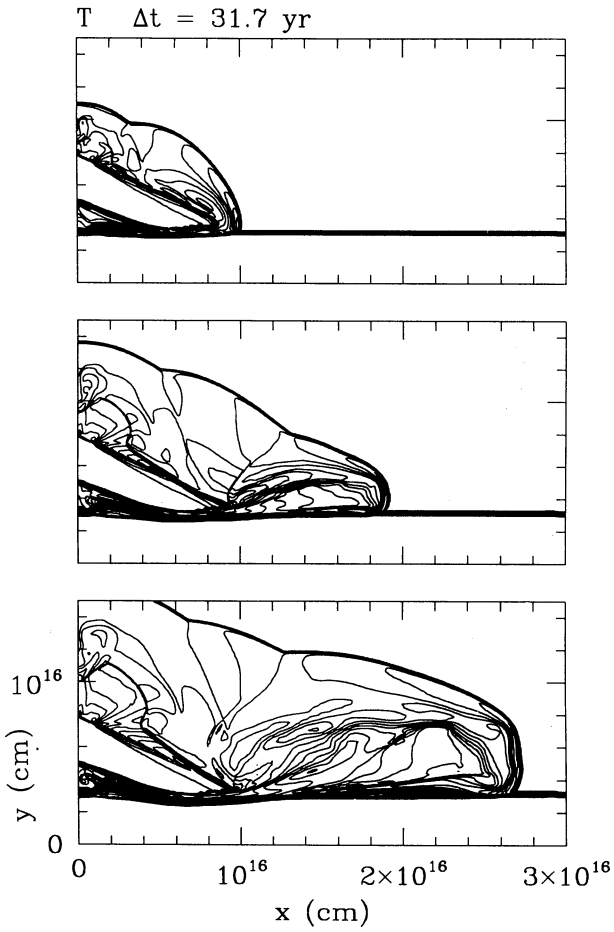

Fig. 10. Time-sequence of the temperature stratification for Model 3 (see the text and Table 1). The successive frames are taken at the same time-intervals as in Figure 9. The logarithmic contours correspond to factors of $\sqrt{2}$.

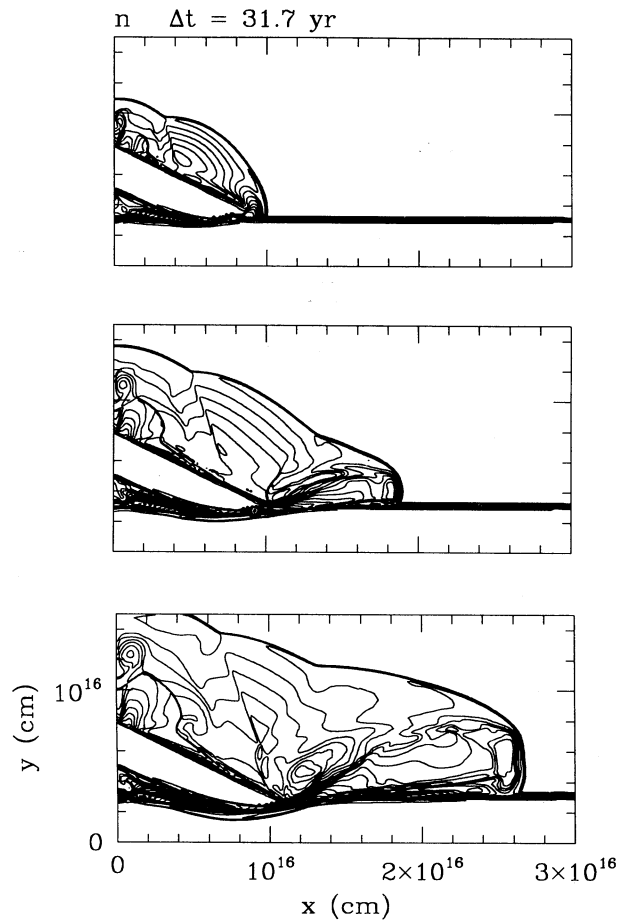

Fig. 11. Time-sequence of the density stratification for Model 4 (see the text and Table 1). The successive frames are taken at time-intervals of 31.7 yr from the beginning of the numerical integration. The logarithmic contours correspond to factors of $\sqrt{2}$.

the two-shock internal working surfaces are still present in the region downstream of the jet/cloud collision. This result is also clearly seen in the [S II] 6717+31 emission coefficient maps shown in Figure 8. The internal working surfaces are seen as emitting knots in the region before the jet/cloud collision, and are also seen as somewhat broader emission features in the downstream region.

It is interesting to note that the spacing between successive internal working surfaces becomes smaller by a factor of ~ 0.9 after the jet beam goes through the $S1$ shock (see Figures 1 and 5). This change in the spacing is consistent with the decrease of the jet beam velocity predicted by equation 4. It is also interesting to note that the separation between the two shocks of each working surface grows quite substantially after the passage through the $S1$ shock, an effect which directly results from the strong increase in the pressure of the gas trapped between the working surface shock pairs.

5. THE COLLISION OF A JET WITH A FINITE DENSITY OBSTACLE

In this section we consider the problem of a jet impacting on a cloud of finite density (an infinite cloud density ρ_c was assumed in §§ 3–4). We present results from two numerical simulations, Models 3 and 4, corresponding to cloud-to-jet density ratios $\rho_c/\rho_j = 1000$ and 100, respectively (see Table 1). In both cases, it has been assumed that the cloud has a depth-independent density, and that it is in pressure equilibrium with a low density surrounding environment. The interface between the cloud and the surrounding environment is assumed to be in-

© Universidad Nacional Autónoma de México • Provided by the NASA Astrophysics Data System

1995RMxAA..31...51R

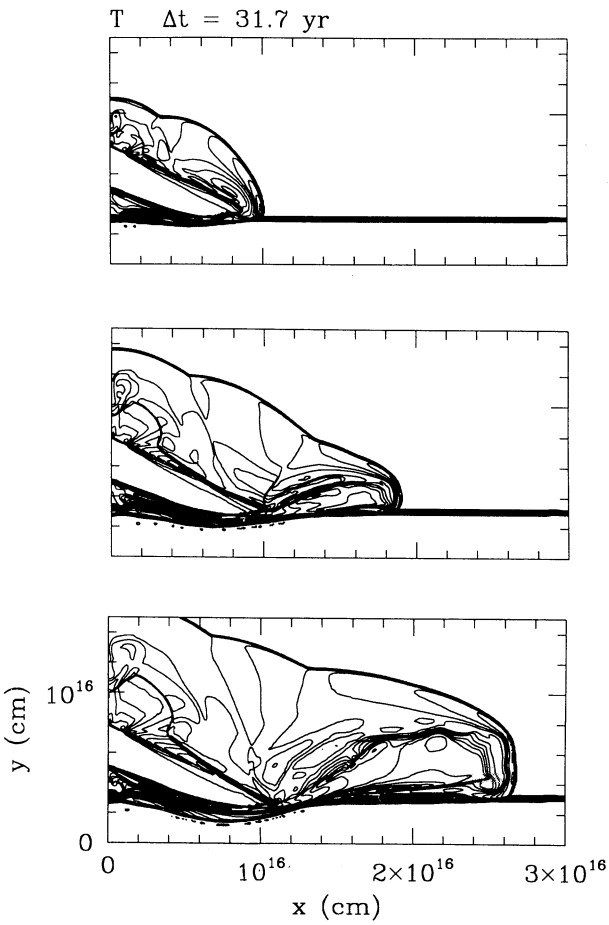

Fig. 12. Time-sequence of the temperature stratification for Model 4 (see the text and Table 1). The successive frames are taken at the same time-intervals as in Figure 11. The logarithmic contours correspond to factors of $\sqrt{2}$.

finitely sharp (i.e., at the resolution of the numerical simulations).

The Model 3 density and temperature time-sequences of Figures 9 and 10 (respectively) show the presence of the $S2$ shock (also see Figure 1) which slowly travels into the dense cloud. The velocity of the $S2$ shock is clearly much larger in the lower cloud-to-jet density contrast Model 4 (see Figures 11 and 12), as is expected from the analytic discussion of § 2 (see equation 1).

The presence of this second $S2$ shock leads to the following interesting effects. For example, at the later evolutionary time of the Model 4 time-sequence (corresponding to an integration time of 95.1 yr, see Figures 11 and 12), the distance travelled by the $S2$ shock (into the dense cloud) is starting to become comparable to the width h_j of the jet beam (see Figure 1). A blow-up of the jet/cloud collision region (see Figure 13) shows that this leads to an appreciable curvature of both the $S1$ shock and the jet/dense cloud contact discontinuity.

The presence of this "hole" in the dense cloud (that is being drilled by the jet) leads to a further deflection of the jet, which now leaves the jet/cloud collision region directed upwards, away from the surface of the cloud (see Figure 13). This has the interesting effect of increasing the angle of deflection of the jet as a function of time, reaching values that are substantially higher than the incidence angle θ (see Figures 11 and 12).

However, as the jet advances into the cloud, the $S1$ shock will become more and more perpendicular to the direction of the flow in the unperturbed jet. Eventually, the flow behind the $S1$ shock will be subsonic, and a well defined bow shock running directly into the cloud will be established. Actually, the $S2$ shock (see Figure 1) can be regarded as the early stages of the development of this bow shock. When the $S1$ shock has become perpendicular to the jet beam and the $S2$ shock has developed into a full bow-shock, the jet will then start to directly penetrate the dense obstacle, and the "deflected jet beam" (seen in our numerical simulations) will effectively disappear.

One can estimate the lifetime t_c of the transitory existence of the jet deflection effect as the time that the $S2$ shock will take to travel a distance of the order of the width h_j of the jet. In other words, we have

$$t_c \sim \sqrt{\frac{\rho_c}{\rho_j}}\,\frac{h_j}{v_j \sin\theta}\,. \tag{8}$$

For the parameters of Model 4 (see Table 1), we would then estimate that the jet will be deflected by the interaction with the dense obstacle for a time $t_c \sim 225$ yr, and will then start to penetrate the cloud with no major change in direction. The jet deflection regime will last a factor of ~ 3 longer for the higher cloud-to-jet density contrast Model 3.

It is hard to compute numerically the precise value of t_c (at which the jet begins to penetrate directly into the dense cloud), since the effect of ablation of cloud material by the jet will play an important role, and also a three-dimensional calculation would actually be necessary. However, we have continued the time-integration of Model 4 beyond $t = 95.1$ yr (see Figures 12 and 13) at twice the spatial resolution (see Table 1), and find that the deflected jet beam starts to pinch off at a time $t_c \sim 130$ yr. The pressure and velocity fields at this time are shown in Figure 14.

In other words, in our numerical simulation we obtain a value of t_c that is roughly two times shorter than the value obtained from equation (8) for the same model parameters. This discrepancy is probably a measure of the uncertainty of the simple es-

© Universidad Nacional Autónoma de México • Provided by the NASA Astrophysics Data System

1995RMxAA..31...51R

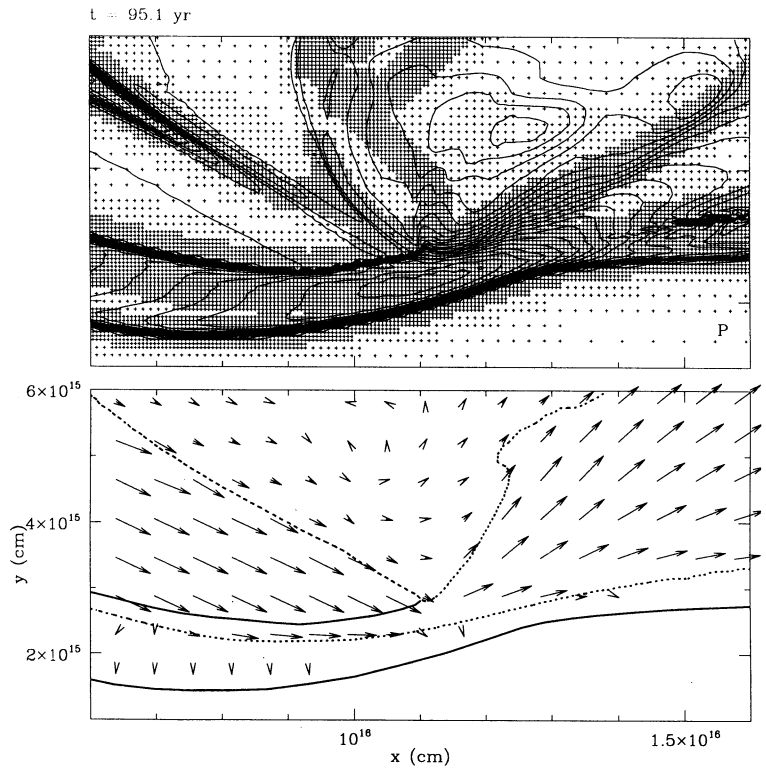

Fig. 13. Blow-up of the jet/cloud interaction region showing the stratification obtained from Model 4 for a time-integration of $t = 95.1$ yr. The top graph shows the pressure contours (factor of $\sqrt{2}$ contours) superimposed on the computational grid resulting from the adaptive grid algorithm. The bottom graph shows the velocity field (only velocities larger than 10 km s^{-1} are shown, and the largest arrows correspond to a velocity of 100 km s^{-1}). In this bottom graph, we have also plotted the jet/cloud and jet/surrounding environment contact discontinuities (dotted lines) as well as the positions of the $S1$ and $S2$ shocks (solid lines, also see Figure 1).

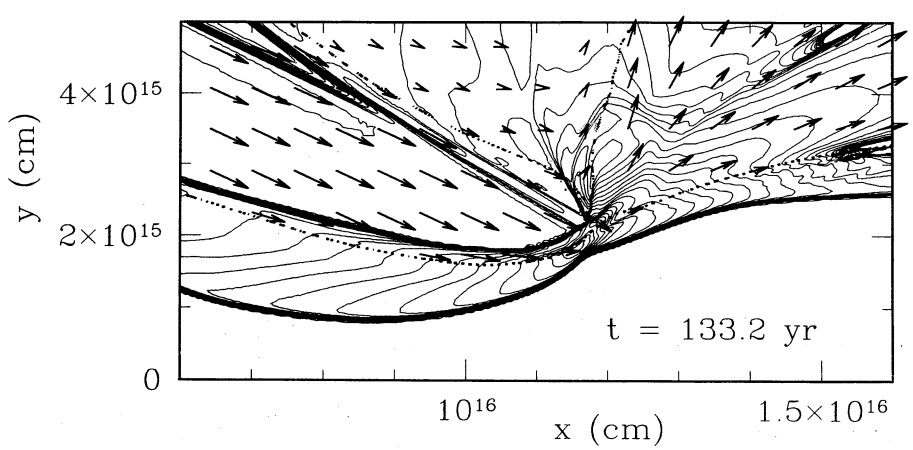

Fig. 14. Blow-up of the jet/cloud interaction region showing the stratification obtained from Model 4 for a time-integration of $t = 133.2$ yr. The solid lines are pressure contours (factor of $\sqrt{2}$ contours), and the dotted lines show the contact discontinuities at the edges of the jet beam. The arrows represent the velocity field (only velocities larger than 10 km s^{-1} are shown, and the largest arrows correspond to a velocity of 100 km s^{-1}). This graph shows the end of the time period over which the collision leads to a deflection of the jet. At this time, the deflected jet beam is being pinched off, and the $S2$ shock (see Fig. 1) is starting to become the bowshock at the new head of the jet (that penetrates directly into the dense cloud).

© Universidad Nacional Autónoma de México • Provided by the NASA Astrophysics Data System

1995RMxAA..31...51R

imate of t_c embodied by equation (8), and can be understood by noting the strong curvature that the S2 shock develops in the numerical simulation (see Figures 1 and 14). This curvature has been neglected in the derivation of equation (8).

6. CONCLUSIONS

This paper discusses an aplication of the analytic formulation of Cantó et al. (1988) to the case of the impact of a jet on a dense cloud. Numerical, radiative "slab jet" simulations are also carried out to confirm this simple, analytic formulation, as well as to extend the model to the case of finite cloud-to-jet density ratios.

Models of the impact of a jet against a rigid surface (which is equivalent to having an infinite density cloud) agree well with the analytic description. An exploration of the effects of a source velocity time-variability shows that the emitting knots (which correspond to the successive internal working surfaces formed along the beam of the jet) survive the jet/cloud collision, and are still seen as coherent entities at larger distances from the source.

We have also computed jet/cloud collisions for finite cloud-to-jet density contrasts. At large enough timescales, the jet starts to drill a curved cavity on the surface of the cloud. In its turn, this curved cavity has the effect of increasing the angle by which the jet is deflected. This effect is estimated to last for the time necessary for the jet to drill a cavity with a depth of the order of a few times the width of the jet beam. At larger timescales, the deflection of the jet will effectively choke off, and the jet will slowly penetrate directly into the dense cloud.

We find that the primary effects of a radiative jet/cloud collision are to deflect the jet to a direction roughly parallel to the surface of the cloud, to decrease the velocity, and to increase the opening angle of the jet beam. It is interesting to note that some HH jets do show such properties.

For example, HH 110 (Reipurth, Heathcote, & Raga 1995) does appear to have a sharp deflection. A clear decrease in the proper motion of the knots and an increase in the opening angle also occurs at the point of deflection. Furthermore, this deflection point appears to spatially coincide with the location of the edge of a molecular cloud core. These properties clearly make HH 110 an interesting candidate for a possible interpretation in terms of the jet/cloud interaction models presented in this paper.

The main limitation of our model is that it refers only to the early evolution of a jet/cloud collision. At later times, other effects will be introduced by the stratification of the cloud (which will be important when the jet bores into the cloud for a number of pressure scale heights), and by the fact that the perturbed cloud material will close back, enclosing the jet beam. This latter process is particularly difficult to model because it is a clearly three-dimensional effect, and will be absent in our two-dimensional, "slab jet" simulations. In future papers, we will study in detail the later stages of the evolution of such an interaction.

We would like to thank an anonymous referee for very helpful comments on this work.

REFERENCES

Cantó, J., & Raga, A.C. 1991, ApJ, 372, 646
Cantó, J., Raga, A.C., & Binette, L. 1989, RevMexAA, 17, 65
Cantó, J., Tenorio-Tagle, G., & Różyczka, M. 1988, A&A, 192, 287
Raga, A.C. 1993, Ap&SS, 208, 163
_____. 1994, in Stellar and Circumstellar Astrophysics, ed. G. Wallerstein & A. Noriega-Crespo, ASP Conf. Ser. 57, p. 85
Raga, A.C., Cantó, J., Binette, L., & Calvet, N. 1990, ApJ, 364, 601
Raga, A.C., Taylor, S., Cabrit, S., & Biro, S. 1995, A&A, in press
Reipurth, B., Raga, A.C., & Heathcote, S. 1995, A&A, submitted
Stone, J., & Norman, M.L. 1993, ApJ, 413, 210

Jorge Cantó and Alejandro C. Raga: Instituto de Astronomía, UNAM, Apartado Postal 70-264, 04510 México, D.F., México. (raga@astroscu.unam.mx).

© Universidad Nacional Autónoma de México • Provided by the NASA Astrophysics Data System